International Journal of Computational Methods and Experimental Measurements
https://www.acadlore.com/journals/IJCMEM

Hydrothermal Analysis of Forced Convection Heat Transfer in an Innovative Tank Heat Exchanger

Ibrahim A. Mahmood[1,2], Tamadher Alnasser[3], Louay A. Mahdi[4], Abdulrazzak Akroot[1], Hasanain A. Abdul Wahhab[5*]

[1] Department of Mechanical Engineering, Faculty of Engineering, Karabuk University, 78050 Karabuk, Turkey
[2] College of Technical Engineering, Al-Farahidi University, 35057 Baghdad, Iraq
[3] Mechanical Engineering Department, University of Technology-Iraq, 35050 Baghdad, Iraq
[4] Energy and Renewable Energies Technology Center, University of Technology-Iraq, 35050 Baghdad, Iraq
[5] Training and Workshop Centre, University of Technology-Iraq, 35050 Baghdad, Iraq

[*] Correspondence: Hasanain A. Abdul Wahhab (20085@uotechnology.edu.iq)

Received: 11-28-2024 **Revised:** 05-03-2025 **Accepted:** 05-09-2025

Citation: I. A. Mahmood, T. Alnasser, L. A. Mahdi, A. Akroot, and H. A. A. Wahhab, "Hydrothermal analysis of forced convection heat transfer in an innovative tank heat exchanger," *Int. J. Comput. Methods Exp. Meas.*, vol. 13, no. 3, pp. 697–708, 2025. https://doi.org/10.56578/ijcmem130317.

Abstract: Heating elements in a circular cross section are mostly utilized as the foundation of heat exchangers because of their simplicity and low production cost. Streamlined circular heaters may separate and create significant wakes, which can result in high-pressure drops. So, they have a much lower hydraulic area and thus need less pumping power. In the context of this research, the main objective is to experimentally investigate the hydrothermal parameters in a water tank heat exchanger heated by new heating fluid supply method. Several heat fluxes were studied during the experiment, and several parameters were considered, such as surface temperature, pumping power, heat flux, Reynolds number, and the average Nusselt. The correlations between those parameters have been developed and analyzed. The values of the Nusselt number change at any change in the Reynolds number, the power of tubular heaters, or the place of the heated cylinder inside the tank. A quasi-linear relationship between pumping power and pressure drop shows that for all heated cylinders in the Re range of $154.34 \leq \mathrm{ReD} \leq 212.51$, the range of mean pumping power was $0.54 \times 10^{-4} \leq \mathrm{Wp} \leq 4.9 \times 10^{-4}$.

Keywords: Forced convection; Heat transfer; Tank heat exchanger; Vertical long heated cylinders

1 Introduction

Heat is transferred either inside the systems themselves or between the systems and their surroundings whenever there is a temperature differential between two different systems. When it comes to transferring thermal energy from a heat source, the appropriate method must be chosen, which is in harmony with the nature of the application. It is frequently possible to explore the various heat transmission techniques autonomously, and the data gathered can then be combined to calculate the overall quantity of heat transferred by system [1, 2]. On the other hand, to successfully remove heat from a system, it is sometimes necessary to use various heat transfer strategies [3, 4]. A wide range of business types operate the forced convection method to enhance their operations [5]. Given how frequently forced heat transfer by convection is employed in industrial settings, it is imperative to show how water velocity affects the coefficients for forced convection heat transfer. Readings of the temperature taken from the vertical plane of a heating material are required for the procedure to be considered complete [6, 7]. Several works have investigated through the use of experiments how heat is distributed through the use of forced convection [8, 9]. In the context of the transmission of heat, this is being done in order to investigate the connection that exists between the Reynolds number and the Nusselt number. The convective heat transfer coefficients have been shown to have a close relationship with one another. Additionally, currently available experimental data are compared [10].

When compared to their counterparts on the outside, the problems associated with convention on the inside have received less attention from researchers [11]. This is a direct result of the preeminent significance of external flows in operational practice. An approach based on the calculation of heat transfer in an analogous tube with a circular

cross-section can be used to estimate the amount of heat transfer that occurs in tubes with a cross-section that is not a circle [12].

In forced convective heat transfer, an outside force, such as a fan or pump, causes fluid or air to move. The heat transmission rate is faster with forced convection than with natural convection [13]. The effects of Re = 40 and Re = 80 on the results of unsteady forced and natural convection heat transfer from horizontal circular and elliptic tubes were studied by Talmor and Seyed-Yagoobi [14]. The two-dimensional Navier-Stokes and energy equations were numerically solved after a detailed experimental thermal field analysis. Wang and Zhou [15] evaluated the air-flow behavior and heat transfer characteristics for two different elliptic tube axis ratios, 1/2 and 1/3. Angles of attack between 0 and 90 degrees were considered, with the Reynolds number varying from 8,000 to 79,000 times. They found that a separation angle of 60 to 90 degrees was optimal to maximize the average heat transfer coefficient. This proved to be the case when they looked at the data. They found that the elliptical tube's minimum means heat transfer rate was higher than the circular tube's. Han and Wright [16] found that when two elliptical tubes with an axis ratio of 0.5 are placed next to one another and subjected to crossflow, the local heat transfer coefficient is significantly affected by the angle of attack and tubes spacing. The shell side of an oval tube bank reduces pressure and improves heat transfer, as reported by Cavazzuti [17]. They found that the frontal areas of shell-side heat exchangers were significantly smaller for oval-tubed designs than for circular-tubed designs. Chaudhry [18] presented the operation of elliptical finned tubes using forced convection. Various Reynolds numbers, from 4 to 103, were assessed experimentally to learn more about heat transfer's unique qualities at each level.

Neuberger et al. [19] found that pressure and heat transfer were reduced when the flow was perpendicular to the airfoil. Compared to a round tube, the Stanton numbers to pressure failure criterion were higher when the NACA-0024 was used as the air-foil test section. A sphere tube was used as a standard for comparison. Heat transfer coefficients for forced convection in several cases of tubes immersed in a moving fluid environment at different conditions were reported [19]. The effects of the Reynolds number on the results of unsteady forced and natural convection heat transfer from horizontal and vertical circular and elliptic tubes were studied by Xia et al. [20]. They calculated free convection from isothermal horizontal elliptic tubes. In both cases, full conservation equations of mass, momentum, and energy had to be solved before any boundary-layer simplifications could be made. They solved free convection from an ellipsoidal tube for Rayleigh numbers between 10 and 103 and axis ratios between 0.1 and 0.964. Specifically, Storrs Hall [21] compared one-row tubes with plate-fin heat exchangers that were either elliptical or circular. There was a notable improvement in efficiency with elliptical tubes. Compared to circular tubes, heat transfer is increased by 18% when using elliptical tubes. Popoola and Ogunlade [22] described forced convection heat transfer in an isentropic, cross flowing elliptical tube. The range of Reynolds number and angle of attack studied in this article was from zero to ninety degrees and two thousand. Between 0.4 and 0.9, tube axis ratios are possible. According to the results, heat transfer is quickest at zero degrees and slowest at ninety degrees [23].

CFD techniques and experimental methods are complex to test the heat transfer and flow distribution in the difficult parallel flow system with many heat transfer systems, this requires large economic costs and a long period [24]. In two-phase flow modeling of simple multi-channel heat exchangers, it requires a long computational period due to the difficulty of capturing and defining the phase interface, which complicates the design of a two-phase flow heat exchanger [25]. Thus, an accurate and rapid method is required to determine the heat transfer and two-phase flow distribution in the parallel flow regime of the heat exchanger design. Camilleri et al. [26] presented a model for investigating the flow distribution of compact heat exchangers based on Kirchhoff's law and used the channel-to-headspace ratio to explain the flow distribution. Bava et al. [27] developed a flow network system to numerically investigate the flow distribution in channel networks. García-Guendulain et al. [28] suggested a mathematical model to study the uniform flow in a flat collector using the mass and momentum conservation equations. More so, they developed a mathematical model to analyze the flow features in collector networks when the tube-to-header area ratio is less than 0.25. Gungor and Winterton [29] reported a modular for single-phase flow distribution in the flat collector using pressure drop correlations. They described that turbulent flow in the tip can develop flow misdistribution. Hu et al. [30] suggested a simulated model for heat exchangers that have multi-port considering phase distribution in the tip. Huang et al. [31] reported a theoretical process to describe the flow distribution in proton exchange membrane fuel cell stacks using the flow network technique, and the effect of two-phase flow in the unit cell on the flow distribution was quantitatively studied [32]. Klugmann et al. [33] studied a numerical model to predict the transient flow distribution of two-phase flow by MATLAB Simulation, but they did not consider the effect of headers. Kumar et al. [34] improved a new model to predict liquid and vapor mass flow rates in each branch of the condenser based on the flow pattern in the header. However, the effect of unequal heating on flow distribution wasn't discussed in their investigation.

Ali et al. [35] introduced a novel empirical correlation designed to predict the overall heat transfer coefficient in concentric tube heat exchangers. The study used a comprehensive dataset of 2700 data points from CFD simulations, examining the impact of critical variables, including hot and cold fluid Reynolds numbers. Jasim et al. [36] studied the impact of the type of hybrid nanofluid on the hydrothermal behavior of the proposed heat exchanger. The volume

concentration of the nanoparticles was a wide range. The results obtained from the different heat transfer fluids considered the Water/MgO-TiO_2 model shows the most outstanding value of thermal performance in all the Reynolds numbers studied. Also, the numerical results obtained show that the use of the proposed double coil tube leads to an increase in the heat transfer rate.

The main objective of this study is to characterize the effect of different heat fluxes on the transfer of heat via forced convection. It was investigated using three heated cylinders as part of a nine-cylinder assembly submerged in water. The effects of forced convection are investigated using three thin cylinders vertically stacked. The fluid is forced to pass through between these cylinders by a differential in pressure, which is also sometimes referred to as an external push (in case of transfer of liquid by pump). In these new investigations on vertically thin cylinders, they discovered that the experimental findings were in good accord with research that had been conducted in the past.

2 Experimental Implementations

The experimental setup aims to investigate forced convection heat transfer from three hot, thin vertical heating elements submerged in water at various heat fluxes. The test rig was built with a stainless steel tank, aluminum heated cylinders, tie rods between the covers of the cylinders, and a water pump. In addition, a set of measuring instruments have been installed to acquire the data of the research variables.

Vertically submerging the assembly cylinders in the direction of gravity required the employment of a stationary water tank that measured $42 \times 42 \times 120$ cm. After forcing water through the inlet hole in the bottom by the pump (by rubber pipe), cold water flows into a stainless-steel cylinder. The cylinder consists of 9 thin vertical cylinders; three contained heaters and temperature sensors made from stainless steel, and 6 were empty and made from aluminum for further future investigations. The pump pushes the water that enters the inlet hole. One of the heater's wires was linked to a digital clamp-on multimeter by a variac, as shown in Figure 1, allowing the user to control the input voltage flowing into the device. Thermocouple wires were linked to a digital temperature recorder so that the thermocouples could read temperatures. During the experiments, heaters were tested at a variety of power levels by monitoring the voltage that was being produced across the heaters by using the variable AC current source. Three different routes were used to produce a wide range of Reynolds numbers. The gate valve controls the flow rate and is adjustable to three flow rates of 32.5, 25, and 15.6 L/min. A water flow sensor was used to display the flow rate to us. The input power of the heater was calculated using the measured current, I (amp), and voltage, V. Thermocouple, and input power values were measured to analyze the steady-state heat transfer caused by forced convection within a boundary condition characterized by a constant heat flow.

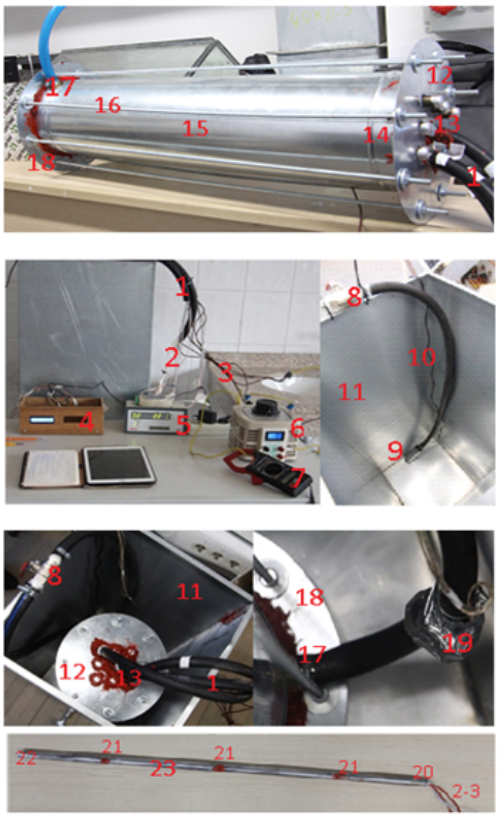

Figure 1. Identification of the experimental setup parts and the measuring instruments

2.1 Design and Fabrication of Thin Vertical Heated Cylinders

The heat exchanger system contains an inner cylinder installed inside a square cross section tank. The inner cylinder is made of stainless steel tubes, with an average thickness of 1.25 mm. The cylinder is 900 mm long and has an outside diameter of 200 mm. The cylinder had three evenly spaced holes bored into its interior. From the bottom up, the distance between the holes is 200 mm, 450 mm, and 700 mm. Fiber glass-insulated, thin thermocouple wires of type-K were inserted through the into the inner side of the cylinder wall. After that, the wires were readjusted so that their ends remained flush with the cylinder's exterior. A tubular heater of identical length to the stainless-steel cylinder was inserted inside of it to provide heat, as shown in Figure 2. Magnesium oxide insulated the area between the cylinder and the tubular heater (MgO). To prevent water from leaking into the cylinder, it used thermal silicon sealant to plug the holes in the cylinder. The 19 mm rubber pipe was used to house the electric and thermocouple wires, as shown in Figure 2.

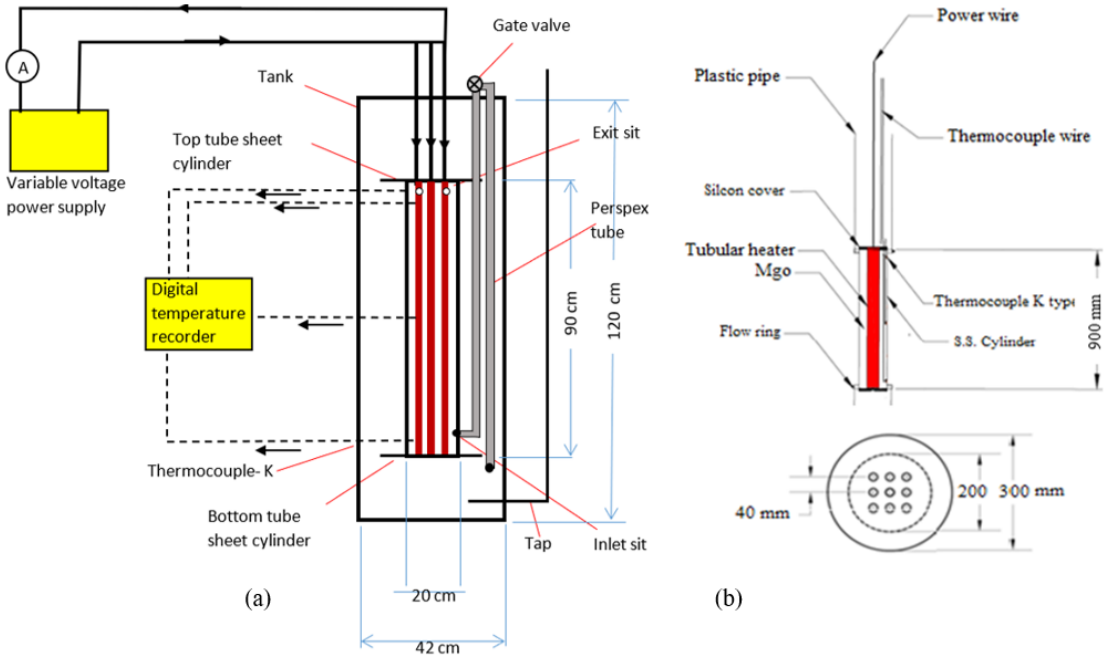

Figure 2. Side and top block diagram view the schematic diagram of the experimental setup for the cylinder and side view for the tubular heater

The Models and Properties of the equipment of the experiment setup and the measurement instruments are seen in Table 1.

Table 1. Technical specifications of setup equipment and measurement instruments

Devices	Model and Properties
Pump	Gross Fluid Transfer Pump 12-volt DC, 40 W
Wattmeter	Energy Consumption Meter Measuring Socket 230V-3680W-16A
Data logger	Elimko Model E-680 Data logger, Working ranges 20 to 75℃ -25-200 V AC, Standard working limits −200 + 1300℃
Water flow sensor	1–60 L/min DC 5-24 V Hall Effect Water Flow Sensor
Stainless steel	16 BWG SS 304L
Thermocouple	Type-K (copper constantan) with tips, fiberglass insulation −75℃ to + 260℃, Length 1.6 m
Variac	Input 220 V, output 0–250 V, 50–60 HZ, max. 4.5 A
Clamp meter	Dt-266 Pens clamp Amperemeter (Multimeter, Avometer)

2.2 Configuration of Stainless Steel Cylinder Assembly

A three-by-three array with a distance between the centers of two cylinders and a diameter ratio ST/D of 2 was created. By employing two circular tube sheets, one on top and one on bottom, with holes for tie rods and cylinders,

an ST/D ratio of 2 was created. The same cylinder configuration was preserved; the placement of eight tie rods at the tube sheet corners is shown in Figure 2, and the assembly was housed inside a stainless steel cylindrical container. Tie rods are solid steel rods used to maintain the spacing between the top and bottom tube sheets at the same level. This container had an outside diameter of 200 mm, an inlet 20 mm diameter hole at the bottom, and four exit holes at the top, each with a diameter of 10 mm, as shown in Figure 2, vertically aligned cylindrical assemblies were submerged in water and aligned with gravity. Galvanized steel was used to build the water tank, as depicted in Figure 2, while Figure 1 demonstrates how the cylinders are positioned around the central cylinder and present the cylinder nomenclature. The surface temperatures of the assembly's three cylinders (the middle and side cylinders) were selected for measurement. Each of the three cylinders received a heating element as part of the installation. In addition, thermocouples were fastened so that the inlet and outlet temperature of the water could be measured at the length of the container cylinder.

2.3 Data Acquisition

A cylinder assembly attached to a variable voltage regulator can be seen vertically installed in the tank. The variac supplied the cylinder heater with variable power ranging from 3.5 to 840 watts while maintaining the voltage. After fifteen minutes, it was noted that the surface temperatures were moving closer and closer to a condition of steady state, as indicated by the digital temperature. The tests were performed on nine uniform heat fluxes of 14.75, 206.4, 663.48, 1,179.52, 1,990.44, 2,830.85, 3,818.71, and 4,954 W/m^2, and the first value was not used in calculations because it was so small. A pump is installed on the exterior of the cylinder container to gather all the cylinders. This pump pulls liquid from the tank's bottom and injects it into the cylinder from the bottom. In addition, a miniature water flow sensor is constructed on the main cylinder's exterior that houses all the cylinders. It is essential to extract the Reynolds numbers, just before the liquid enters the cylinder that measures the flow rate of the liquid. A gate valve was inserted between the water flow sensor and the pump and measured three different flows by adjusting the amount of opening that the gate valve allowed to widen the scope of this study. When it was opened for the first time, the valve was fully open; when it was opened for the second and third times, it was partially open. The following effect was brought about by the three different flow rates: 15.6, 25, and 32.5 L/min. The surface temperature changes along the vertical cylinders are measured. They can be seen at various axial distances from the bottom side and for various flow rates.

3 Theoretical Analysis

The two-dimensional Navier-Stokes and energy equations were mathematically solved after a detailed experimental thermal field analysis. Total heat transfer [37–41] from a thin vertical cylinder can be calculated as:

$$Q = Q_{cond} = \dot{Q}_{conv} + Q_{rad} \tag{1}$$

Calculating the amount of heat transferred by conduction can really be done using Fourier's law, Eq. (2).

$$Q_{cond} = -kA\frac{\partial T}{\partial x} \tag{2}$$

where, k is magnesium oxide's (MgO) thermal conductivity, the heat transfer area is A, and the temperature gradient or temperature profile's slope is dT/dx. As will be seen in the following section, the conduction of heat can occur in this scenario at one of three different points:

Transfer of heat from an external heat source to the surfaces of stainless steel cylinders: It is difficult to measure the surface temperature of the tubular heater while it is contained within a stainless steel cylinder and also because the distance between the tubular heater and the cylinder is minimal and filled with MgO, which has 30 W/m·°C thermal conductivity, the conduction losses that occur between the tubular heater and the stainless steel cylinder are disregarded. The temperature difference between the end of the heater and the cylinders equals zero. So, the top and bottom ceramic pipes do not get any heat from the tubular heater. Calculations for heat transmission by radiation from a stainless-steel cylinder's surface are as follows:

$$Q_{\text{rad}} = \varepsilon A\sigma F\left(T_{\text{sav}}^4 - T_m^4\right) \tag{3}$$

where, ε is the worn stainless steel's emissivity, σ is the Stefan Boltzmann constant σ = 5.66 ×10^{-8} W/m^2·K^4, F is the shape factor, T_{sav} is the cylinder's average surface temperature, and T_m is the water's mean temperature in Kelvin.

Radiation-related heat transfer was calculated at typical temperatures and determined to account for less than 3 percent of all heat transfer; hence, it is disregarded. Since it was shown that convection transfers nearly 97 percent

of the total heat to the fluid. Eq. (1) can be condensed to the following by ignoring the losses in heat transmission caused by conduction and radiation heat transfer [37].

$$\dot{Q}_{\text{conv}} = hA_{\text{S}}\left(T_e - T_{\text{in}}\right) \tag{4}$$

According to Jasim et al. [36] and more, the physical characteristics of water are computed at mean temperature, Tm and average surface temperatures, T_{sav} by Eq. (5) and Eq. (6):

$$T_m = \frac{T_{in} + T_e}{2} \tag{5}$$

$$T_{\text{sav}} = \frac{T_{S1} + T_{S2} + T_{S3}}{3} \tag{6}$$

where, μ, Pr, Pr_s from Mangrulkar et al. [37], also the value of the density of water (ρ) was constant at 998.23 kg/m^3 at 1.0 atm [39]. The viscosity (μ_x) was the extracted value used in solving mathematics and making curves. The Average Reynold number was calculated by Eq. (7) as follows [38, 39]:

$$Re_D = \frac{\rho V_{\max} D}{\mu} \tag{7}$$

$$V_{\max} = \frac{s_T}{s_T - D} V \tag{8}$$

$$V = \frac{\dot{V}}{(N_T S_T L)} \tag{9}$$

The following steps were taken to arrive at the Average Nusselt Number by Eq. (10):

$$Nu_D = \frac{hD}{K_f} = C\,\mathrm{Re}_D^m\,\mathrm{Pr}^n\left(\mathrm{Pr}\,/\,\mathrm{Pr}_s\right)^{0.25} \tag{10}$$

$$Nu_{D,NL} = \mathrm{F} Nu_D \tag{11}$$

The parameters C, m, n, and F are constants. Where the heat flux was determined by Eq. (12):

$$q'' = \frac{P}{A_S} \tag{12}$$

$$P = I * V \tag{13}$$

$$A_S = N\pi DL \tag{14}$$

The pumping power required can be determined by Eq. (15) and the pressure drop by Eq. (16):

$$\dot{W}_P = \dot{V}\Delta P \tag{15}$$

$$\Delta P = N_L \mathrm{f}\chi \frac{\rho V^2\,\max}{2} \tag{16}$$

4 Uncertainty Analysis

The uncertainty quantifies the expected accuracy, but it is not a guarantee of accuracy. The discrepancy between the measured value and the true value of the quantity, Eq. (17), may arise from different sources.

$$\text{Measured value} = \text{true value} \pm \text{error} \tag{17}$$

Errors could be classified as Bias errors and Random errors. Bias error is a systematic inaccuracy caused by a mechanism that can be (ideally) controlled. Random error is a non-repeatable inaccuracy caused by an unknown or uncontrollable influence [34]. Random errors introduce scatter in the measured values and propagate through the data analysis to produce scatter in values computed from the measurements. Ideally random errors establish the limits on the precision of a measurement, not on the accuracy of a measurement. A more realistic method is to use the root-sum-of-squares method, that is, by taking the square root of the sum of the individual errors [34]. Table 2 shows the uncertainty percentage error of the experimental yield values measured.

$$\delta_{\text{total}} = \left[(\delta \text{ sensor})^2 + (\delta \text{ instrument})^2\right]^{0.5} \tag{18}$$

$$\text{Min.\&Max. Uncer.}(\%) = 100 \times (\delta_{\text{total}}/\text{Min.\&Max. Reading}) \tag{19}$$

Table 2. The uncertainty percentage error of the experimental yield values measured

Parameter	Min. for Recorded Value	Max. for Recorded Value	Uncertainty (%)
Water flow rate	15.6 SLPM	32.5 ALPM	0.46–0.39%
Temperature	32°C	83°C	0.19–0.12%
Voltage	16.4 V	44.4 V	0.54–0.32%
Current	5.4 A	18.9 A	0.63–0.22%

5 Results and Discussion

Results for the middle vertical thin cylinder in water in assembly induced convective heat transfer presented in Figure 3, the delivery of a constant heat flux led to an increase in temperature along the cylinder's axis, with higher surface temperatures at higher fluid flow rates and lower flow rates leading to higher water temperatures at the outlet 0.9 m. This is because heat transfer from the surface of the cylinder will take longer if the water flow rate is low.

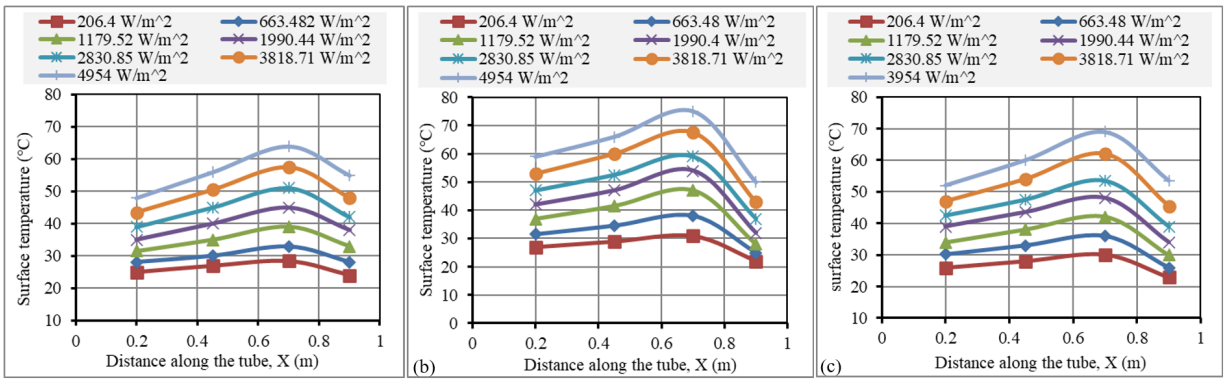

Figure 3. Variations of surface temperature at three axial points and in the outlet in the middle cylinder in the assembly were measured: (a) at 15.6 L/min; (b) at 25 L/min; and (c) at 32.5 L/min

The following explains the distribution's overall shape and pattern: While the surface temperature does increase with increasing axial distance, the temperature has reached its maximum at a distance of x = 700 mm. Surface temperature varies along the cylinder's length for various reasons, the most important of which is the formation of a thermal boundary layer, which can be thought of as a thermal insulator. There are three distinct causes for these temperature shifts: Because laminarization forms along the near wall of the cylinder, the boundary layer thicknesses

start as clearly zero at the beginning of the heated length. This is so because the action moves along the near wall of the cylinder. This resultant situation naturally arises from the cylinder's cylindrical shape. It has been proposed that the surface temperature be raised in small, consistent increments. This is because it follows logically that the regional heat transfer coefficient will fall if the local surface temperature keeps rising. When the heat is dispersed uniformly throughout the cylinder, the water temperature cannot get any higher than it is now. Modifications to the water's physicochemical properties are proportional to the water's temperature. The immediate result is that the temperature can never again increase beyond its current high level. Since less friction is encountered during motion in water with a higher thermal conductivity, and radial flow increases, there will be more friction to the flow of water if its thermal conductivity is lower than that of the viscous water. The viscosity of a liquid can serve as an indicator of its thermal conductivity. The rising boundary layer of hot fluid is radially connected to the cold water. This is due to the rising of the hot boundary layer fluid. This modification will result in a greater rate of local heat conduction. Because of the increased turbulence in this area, the rate at which heat is transferred from the surface of the cylinder to the water is increased. For that, the surface temperature of the cylinder will decrease.

The current results for middle cylinder surface temperatures are compared to those given by Mangrulkar et al. [38], Mohanty et al. [39], and Khalifa and Hussien [40]. The results show that the two sets of data of the middle cylinder are in good agreement. The middle cylinder is where the current, I experience the highest flow rate. Forced convection and natural convection differ in several ways. The most notable of which is the rate at which heat is transferred, as shown in Figure 4. At this point, it begins to decrease due to the turbulent mixing of cold and hot water flowing from hot cylinders and the turbulence formed from the cold water itself.

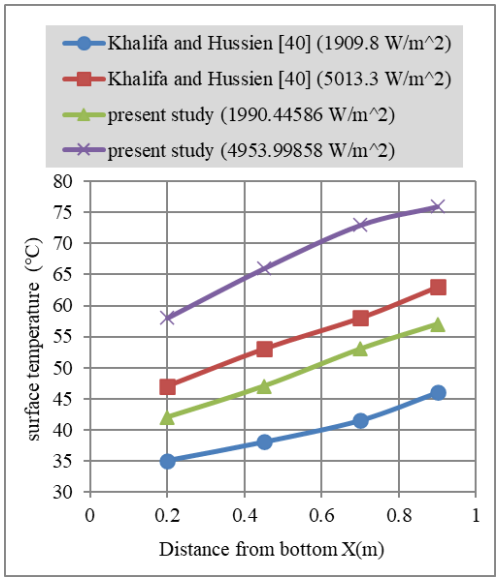

Figure 4. Comparison of Surface temperature at some roughly similar uniform heat flux values of the previous natural convection study for the middle cylinder in the assembly

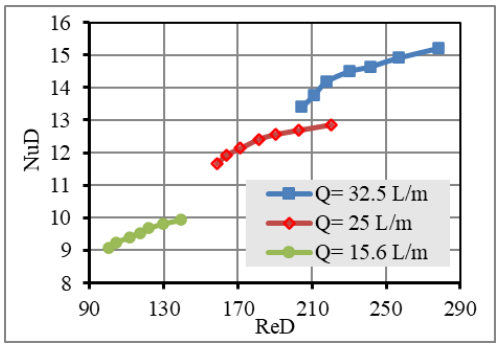

Figure 5. Average Nusselt and average Reynolds numbers at different heat fluxes in different flow rates for the middle cylinder in an assembly

The mean temperature and the average surface temperature were used as a starting point to determine the physical characteristics of the water and the cylinder's surface, which were measured. This was done when determining the

cylinder's surface temperatures, as well as the inlet and outlet water temperatures, as described by Assaf et al. [41]. The Nusselt and Reynolds numbers were utilized to determine whether or not there is a relationship between the technology of forced convection heat transfer and dimensionless local numbers. The findings of this investigation are presented in this section. The results of this study, which evaluated the relationship between the average Nusselt number and the average Reynolds numbers when exposed to a variety of heat flows, led the researchers to the conclusion that the Nusselt number gradually increases with the Reynolds numbers and that empirical associations can be made between the dimensionless numbers of forced convection heat transfer. It was determined for each flow rate within the Re range of $100.31 \leq \text{ReD} \leq 278.14$. The accompanying image provides a visual representation of these results, as shown in Figure 5.

The average Nusselt number and average Reynolds numbers for average flow rates in the range ($154.34 \leq \text{ReD} \leq 212.51$) are also extracted, as shown in Figure 6 with equation $y = 0.0198x + 8.3956$. The quasi-linear relationship had an R^2 of 0.9106; this curve is shown for the side cylinders to compare later with the middle cylinder. The average Nusselt number for flow rates tends to rise with the average Reynolds number when the former increases. It is observed that when the flow rate is reduced, the surface temperatures of the cylinders are lower while the water temperature is higher. This is due to the improvement in heat transfer processes between the cylinder surfaces and the water as the flow rate decreases. The cylinders lose much heat to the water when the water is moving slowly. The surface temperatures of the current study's cylinders are higher than those of the previous research, as shown in Figure 4, because the previous study was working on natural heat transfer, so they did not use a fluid flow pump at all. A complete Nusselt number profile differs for the middle and side cylinders. This discrepancy arises from the expanding turbulence in the region created by the heated cylinders. There is no difference in the range of ReD between different cylinders because the amount of ReD is determined by the viscosity of the water, which in turn is determined by the mean temperature of the water at the inlet and outlet, as well as the fluid flow rate.

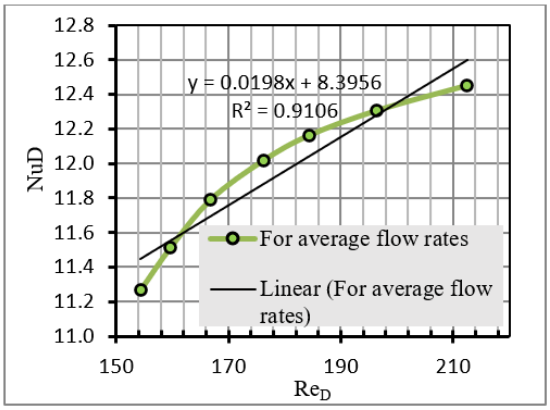

Figure 6. Average Nusselt number and average Reynolds numbers for average flow rates for the side cylinders in an assembly

6 Conclusions

An experimental investigation of forced convection heat transfer was performed in a distinctive design of heat exchanger heating elements in a cylinder immersed in a water tank. The study concludes that, regardless of the heat fluxes used, the overall contour of the surface temperature distribution across the axial distance of the cylinders remains constant. Also, the water on the surface is heated proportionally with an increasing axial distance up to 700 mm. The percentage of heat transfer through radiation was about three percent at the system's highest energy and highest temperature recorded and thus was ignored. It was also concluded that there is a quasi-linear relationship between the Nusselt number and the Reynolds number. For all heated cylinders operating within a range of $154.3 \leq \text{ReD} \leq 212.5$, the range of mean pumping force was $0.54 \times 10^{-4} \leq \text{Wp} \leq 4.9 \times 10^{-4}$. The most important discovered was:

• Water's flow rate effects the heat transfer rate from the surface of the heated cylinders as it decreases when the water flow velocity is raised.

• The surface temperature of the heated cylinders is higher in forced convection compared to natural convection because there is no water flow in natural convection. Also, the average Nusselt number increases as the water flow rate increases.

As recommendation to the future study of the cylinder remaining heat using the same cylinder with the same dimensions; visualizing laminar and turbulent zones with a high-definition thermal camera.

Data Availability

The data used to support the findings of this study are available from the corresponding author upon request.

Acknowledgment

The authors acknowledge University of Technology- Iraq for the support in conducting the research and producing this paper.

Conflicts of Interest

The authors declare that they have no conflicts of interest.

References

[1] I. B. Mansir, R. Ben-Mansour, and M. A. Habib, "Numerical modelling of heat transfer characteristics in a two-pass oxygen transport reactor for fire tube boilers under oxy-fuel combustion," *Appl. Therm. Eng.*, vol. 195, p. 117248, 2021. https://doi.org/10.1016/j.applthermaleng.2021.117248

[2] H. Q. Khafaji, H. A. Abdul Wahhab, S. S. Alsaedi, W. A. K. Al-Maliki, F. Alobaid, and B. Epple, "Thermal performance evaluation of a tubular heat exchanger fitted with combined basket–twisted tape inserts," *Appl. Sci.*, vol. 12, no. 10, p. 4807, 2022. https://doi.org/10.3390/app12104807

[3] Y. Hashim Hussein, A. Akroot, and T. A. Tahseen, "Investigation of free convection heat transfer from vertical cylinders with semicircular fins," *Exp. Heat Transf.*, vol. 37, no. 7, pp. 940–959, 2023. https://doi.org/10.1080/08916152.2023.2240805

[4] S. Bhattacharya, M. K. Verma, and R. Samtaney, "Revisiting Reynolds and Nusselt numbers in turbulent thermal convection," *Phys. Fluids*, vol. 33, no. 1, 2021. https://doi.org/10.1063/5.0032498

[5] Y. Wei, X. Liu, K. Zhu, and Y. Huang, "A unified lattice Boltzmann framework for combined radiation-conduction heat transfer," *Int. J. Heat Mass Transf.*, vol. 200, p. 123513, 2023. https://doi.org/10.1016/j.ijheatmasstransfer.2022.123513

[6] S. Verma, B. R. S. Freeman, and A. Hemmati, "Effects of Reynolds number and average angle of attack on the laminar scaling of oscillating foils," *Phys. Fluids*, vol. 34, no. 3, 2022. https://doi.org/10.1063/5.0082578

[7] H. Zhang, Q. Sun, Z. Sun, and Y. Lu, "Experimental and numerical investigation of electromigration behavior of printed silver wire under high current density," *J. Electron. Packag.*, vol. 145, no. 2, p. 021006, 2023. https://doi.org/10.1115/1.4055469

[8] N. Vučetić, G. Jovičić, R. Antunović, S. Sovilj-Nikić, A. Košarac, and D. Jeremić, "Integrity assessment of an aircraft cylinder assembly with a crack," *Mater. Tehnol.*, vol. 56, no. 4, pp. 389–396, 2022. https://doi.org/10.17222/mit.2022.430

[9] B. Huang, Q. Zhao, C. Sun, L. Zhu, H. Zhang, Y. Zhang, C. Liu, and F. Li, "Trace analysis of gases and liquids with spontaneous Raman scattering based on the integrating sphere principle," *Anal. Chem.*, vol. 94, no. 39, pp. 13 311–13 314, 2022. https://doi.org/10.1021/acs.analchem.2c03701

[10] M. Bdaiwi, A. Akroot, H. A. Abdul Wahhab, Y. H. Assaf, M. Y. Nawaf, and W. Talal, "Enhancement heat exchanger performance by insert dimple surface ball inside tubes: A review," *Results Eng.*, vol. 19, p. 101323, 2023. https://doi.org/10.1016/j.rineng.2023.101323

[11] A. M. Lavasani, T. Maarefdoost, and H. Bayat, "Effect of blockage ratio on pressure drag and heat transfer of a cam-shaped tube," *Heat Mass Transf.*, vol. 52, no. 9, pp. 1935–1942, 2016. https://doi.org/10.1007/s00231-015-1711-3

[12] R. Deepakkumar, S. Jayavel, and S. Tiwari, "Cross flow past circular cylinder with waviness in confining walls near the cylinder," *J. Appl. Fluid Mech.*, vol. 10, no. 1, pp. 183–197, 2017. https://doi.org/10.18869/acadpub.jafm.73.238.26148

[13] A. A. Gholami, M. A. Wahid, and H. A. Mohammed, "Heat transfer enhancement and pressure drop for fin-and-tube compact heat exchangers with wavy rectangular winglet-type vortex generators," *Int. Commun. Heat Mass Transf.*, vol. 54, pp. 132–140, 2014. https://doi.org/10.1016/j.icheatmasstransfer.2014.02.016

[14] M. Talmor and J. Seyed-Yagoobi, "Electrohydrodynamically augmented internal forced convection," in *Handbook of Thermal Science and Engineering*. Cham: Springer International Publishing, 2018, pp. 479–526. https://doi.org/10.1007/978-3-319-26695-4_7

[15] Z. H. Wang and Z. K. Zhou, "External natural convection heat transfer of liquid metal under the influence of the magnetic field," *Int. J. Heat Mass Transf.*, vol. 134, pp. 175–184, 2019. https://doi.org/10.1016/j.ijheatmasstransfer.2018.12.173

[16] J. C. Han and L. Wright, *External Forced Convection*. Boca Raton: CRC Press, 2022.

[17] M. Cavazzuti, "A forced convection application: Surface optimization for enhanced heat transfer." in *Optimization Methods: From Theory to Design Scientific and Technological Aspects in Mechanics*, 2012, pp. 153–173. https://doi.org/10.1007/978-3-642-31187-1_8

[18] M. H. Chaudhry, *Governing Equations for One-Dimensional Flow, Open-Channel Flow*. Springer International Publishing, 2022.

[19] P. Neuberger, R. Adamovský, and M. Šed'ová, "Temperatures and heat flows in a soil enclosing a slinky horizontal heat exchanger," *Energies*, vol. 7, no. 2, pp. 972–987, 2014. https://doi.org/10.3390/en7020972

[20] T. Xia, Y. Han, C. Zhu, Z. Sun, C. Yuan, Q. Cui, J. Cheng, W. Du, W. Li, K. Xie, and et al., "Thermochemical mechanism of optimized lanthanum chromite heaters for high-pressure and high-temperature experiments," *ACS Appl. Mater. Interfaces*, vol. 14, no. 28, pp. 32 244–32 252, 2022. https://doi.org/10.1021/acsami.2c07639

[21] J. Storrs Hall, "VARIAC: An autogenous cognitive architecture," *Front. Artif. Intell. Appl.*, vol. 171, no. 1, pp. 176–187, 2008.

[22] A. I. Popoola and I. I. Ogunlade, "Development and implementation of a controller for 220 volts, 2.5 horsepower liquid pump," *Niger. J. Phys.*, vol. 17S, pp. 269–273, 2005.

[23] S. Hasan Ibrahim and H. A. Abdul Wahhab, "Influence of twisted tape inserts with perforation on heat transfer and pressure drop inside circular tube: Numerical and experimental investigation," in *Proceedings of the International Conference on Production, Energy and Reliability (ICPER 2020)*, 2023, pp. 281–293. https://doi.org/10.1007/978-981-19-1939-8_24

[24] H. Tan, P. Du, K. Zong, G. Meng, X. Gao, and Y. Li, "Investigation on the temperature distribution in the two-phase spider netted microchannel network heat sink with non-uniform heat flux," *Int. J. Therm. Sci.*, vol. 169, p. 107079, 2021. https://doi.org/10.1016/j.ijthermalsci.2021.107079

[25] J. Zhou, M. Ding, H. Bian, Y. Zhang, and Z. Sun, "CFD simulation for the effect of the header match on the flow distribution in a central-type parallel heat exchanger," *Chem. Eng. Res. Des.*, vol. 136, pp. 144–153, 2018. https://doi.org/10.1016/j.cherd.2018.04.047

[26] R. Camilleri, D. A. Howey, and M. D. McCulloch, "Predicting the flow distribution in compact parallel flow heat exchangers," *Appl. Therm. Eng.*, vol. 90, pp. 551–558, 2015. https://doi.org/10.1016/j.applthermaleng.2015.07.002

[27] F. Bava and S. Furbo, "A numerical model for pressure drop and flow distribution in a solar collector with U-connected absorber pipes," *Sol. Energy*, vol. 134, pp. 264–272, 2016. https://doi.org/10.1016/j.solener.2016.05.012

[28] J. M. García-Guendulain, J. M. Riesco-Ávila, and M. Picón-Núñez, "Reducing thermal imbalances and flow nonuniformity in solar collectors through the selection of free flow area ratio," *Energy*, vol. 194, p. 116897, 2020. https://doi.org/10.1016/j.energy.2020.116897

[29] K. E. Gungor and R. H. S. Winterton, "A general correlation for flow boiling in tubes and annuli," *Int. J. Heat Mass Transf.*, vol. 29, no. 3, pp. 351–358, 1986. https://doi.org/10.1016/0017-9310(86)90205-X

[30] C. Hu, R. Wang, P. Yang, W. Ling, M. Zeng, J. Qian, and Q. Wang, "Numerical investigation on two-phase flow heat transfer performance and instability with discrete heat sources in parallel channels," *Energies*, vol. 14, no. 15, p. 4408, 2021. https://doi.org/10.3390/en14154408

[31] F. Huang, D. Qiu, Z. Xu, L. Peng, and X. Lai, "Analysis and improvement of flow distribution in manifold for proton exchange membrane fuel cell stacks," *Energy*, vol. 226, p. 120427, 2021. https://doi.org/10.1016/j.energy.2021.120427

[32] I. E. Idelchik, *Handbook of Hydraulic Resistance*. Begell House, 2008.

[33] M. Klugmann, P. Dabrowski, and D. Mikielewicz, "Flow distribution and heat transfer in minigap and minichannel heat exchangers during flow boiling," *Int. J. Heat Mass Transf.*, vol. 181, p. 116034, 2020. https://doi.org/10.1016/j.applthermaleng.2020.116034

[34] R. Kumar, G. Singh, and D. Mikielewicz, "Effect of asymmetric fluid flow distribution on flow boiling in a microchannel heat sink—An experimental investigation," *Appl. Therm. Eng.*, vol. 213, p. 118710, 2022. https://doi.org/10.1016/j.applthermaleng.2022.118710

[35] S. Ali, J. Faraj, and M. Khaled, "A correlation for U-value for laminar and turbulent flows in concentric tube heat exchangers," *Int. J. Thermofluids*, vol. 23, p. 100797, 2024. https://doi.org/10.1016/j.ijft.2024.100797

[36] D. J. Jasim, O. S. Mahdy, A. Basem, S. H. H. Karouei, and M. Alinia-kolaei, "Hydrothermal analysis of hybrid nanofluid flow inside a shell and double coil heat exchanger; Numerical examination," *Int. J. Thermofluids*, vol. 23, p. 100770, 2024. https://doi.org/10.1016/j.ijft.2024.100770

[37] C. K. Mangrulkar, J. D. Abraham, and A. S. Dhoble, "Numerical studies on the near wall y+ effect on heat and flow characteristics of the cross flow tube bank," *J. Phys. Conf. Ser.*, vol. 1240, p. 012110, 2019. https://doi.org/10.1088/1742-6596/1240/1/012110

[38] C. K. Mangrulkar, A. S. Dhoble, P. K. Pant, N. Kumar, A. Gupta, and S. Chamoli, "Thermal performance escalation of cross flow heat exchanger using in-line elliptical tubes," *Exp. Heat Transf.*, vol. 33, no. 7, pp. 587–612, 2020. https://doi.org/10.1080/08916152.2019.1704946

[39] R. L. Mohanty, A. Swain, and M. K. Das, "Thermal performance of mixed tube bundle composed of circular and elliptical tubes," *Therm. Sci. Eng. Prog.*, vol. 5, pp. 492–505, 2018. https://doi.org/10.1016/j.tsep.2018.02.009

[40] A. J. N. Khalifa and Z. A. Hussien, "Natural convection heat transfer from a single and multiple heated thin cylinders in water," *Heat Mass Transf.*, vol. 51, no. 11, pp. 1579–1586, 2015. https://doi.org/10.1007/s00231-015-1524-4

[41] Y. H. Assaf, A. Akroot, H. A. Abdul Wahhab, W. Talal, M. Bdaiwi, and M. Y. Nawaf, "Impact of nano additives in heat exchangers with twisted tapes and rings to increase efficiency: A review," *Sustainability*, vol. 15, no. 10, p. 7867, 2023. https://doi.org/10.3390/su15107867

Nomenclature

A	Area, m^2
CP	specific heat, $J{\cdot}kg^{-1}{\cdot}K^{-1}$
F	the form factor
k	thermal conductivity, $W{\cdot}m^{-1}.K^{-1}$
Nu	local Nusselt number along the heat source
Q	Total heat transfer, Watt

Greek symbols

α	thermal diffusivity, $m^2{\cdot}s^{-1}$
β	thermal expansion coefficient, K^{-1}
ε	worn stainless steel's emissivity
ρ	density, kg/m^3
μ	dynamic viscosity, $kg{\cdot}m^{-1}{\cdot}s^{-1}$

Subscripts

cond	condaction
conv	convection
rad	radiation